Brazilian Journal of Geophysics (2022) 40(Suppl. 1): 125-140
Brazilian Geophysical Society
ISSN 2764-8044
DOI: 10.22564/brjg.v40i1.2136

HIGHLIGHTS OF SOLAR OBSERVATIONS WITH TWO BRAZILIAN RADIO TELESCOPES

Adriana Valio * Fabian Menezes and Douglas Felix da Silva

[1] Universidade Presbiteriana Mackenzie - UPM, Center for Radio Astronomy and Astrophysics - CRAAM, São Paulo, SP, Brazil

*Corresponding author e-mail: avalio@craam.mackenzie.br

ABSTRACT. Solar radio emission originates from the solar atmosphere, and basically consists of emission from the quiet Sun, active regions, and flares. The slowly varying emission from the quiet solar atmosphere follows the periodicity of the 11-year Solar Activity Cycle. Active regions on the solar surface produce emission that varies on timescale of days or weeks, also known as the quiescent component. Finally, solar bursts are a sudden increase of the emission on timescales of seconds to hours resulting from solar magnetic activity. These three components are produced by different emission mechanisms at distinct radio wavelengths. At microwave and millimeter wavelengths, the quiet Sun emission is produced by bremsstrahlung from thermal electrons. The height on the solar atmosphere where the submillimeter emission is mostly produced was determined to be ≤ 3000 km from center-to-limb observations at multiple radio frequencies. The quiescent radio emission from the active regions, usually brighter than the surrounding solar disk, is dominated by thermal gyroresonance at microwaves and by optically thick thermal bremsstrahlung at millimetric and submillimetric waves. Lastly, gyrosynchrotron radiation from nonthermal electrons is responsible for the flare emission at high radio frequencies. In this review, the discoveries about the Sun obtained from two Brazilian radio telescopes installed at CASLEO (Argentina): the Submillimeter Solar Telescope (SST, 212 and 405 GHz) and the POlarization Emission of Millimeter Solar Activity (POEMAS, 45 and 90 GHz) are presented. The main result from SST was the discovery of a new spectral component increasing toward even higher frequencies.

Keywords: Solar emission, Radio observations, Quiet Sun, Solar active regions, Solar flares

INTRODUCTION

Due to its **distance** to the Sun, **within the Solar System habitable zone**, Earth is capable of sustaining life as we know it, mainly because the solar radiation maintains a comfortable temperature on our planet's surface and our Sun is not too active. Nevertheless, its activity especially in the form of flares and coronal mass ejections sometimes destabilizes Earth's geomagnetic field and technological devices in orbit and on the ground. The impacts resulting from solar activity phenomena are known as Space Weather.

The oldest indicators of solar activity are sunspots, small dark regions commonly seen on the surface of the Sun (Fig. 1). Since 1610, when Galileo and others pointed their primitive telescopes to the Sun, the number of sunspots has been monitored. Nevertheless, there have been reports of sunspots by the Chinese as early as 800 BC. These are regions of strong magnetic fields of approximately 100 to 4000 G (Valio et al., 2020). Sunspots are darker than the surrounding photosphere due to their lower temperature, between 4000 - 5000 K. This occurs because the magnetic field lines within a sunspot obstruct the overturning of the convective cells below the solar surface, which transport energy from the solar interior.

In 1843 Schwabe discovered that sunspot occurrence followed a periodicity of approximately 11 years, which became known as the solar Activity Cycle. Today it is known that not only sunspots follow the 11-year cycle, but also the occurrence of flares (see Figure 19 of Hathaway, 2015) and CMEs (Webb and Howard, 2012). During periods of maximum activity of the Sun, many flares happen, as well as mass

ejections, while during the years of minimum activity very few, if any, of these phenomena occur. Moreover, the X-ray emission from the Sun is higher during solar maxima (Takeda et al., 2019). Currently the Sun is in its rising phase of activity from the minimum which occurred in 2020. The last solar maximum occurred around 2013.

All solar active phenomena occur in the solar atmosphere at or above regions of enhanced magnetic fields. Groups of sunspots are known as active regions. Magnetic loops connect spots of different polarity and traverse the solar atmosphere all the way to the corona. When there is a reconfiguration of the magnetic loops, energy is released. This sudden energy release may produce solar flares and/or mass ejections (Benz, 2008).

A solar flare is a sudden release of energy of the order of 10^{32} erg, which happens in a few seconds or can last for at most an hour (Hudson and Willson, 1983; Emslie et al., 2004). As mentioned above, the energy source is supplied by the magnetic fields within active regions. This energy accelerates particles, ions and electrons, up to energies of MeV, producing copious amounts of radiation, and also heating the local plasma (Heyvaerts et al., 1977; Melrose, 1990). This hot plasma fills the magnetic loops which become bright in X-rays. A flare is a complex phenomenon in which several magnetic loops may be involved (Kerr, 2022).

Another type of activity phenomenon is coronal mass ejection (CME), when $10^{15} - 10^{16}$ g of matter (electrons, protons, and ions) wrapped into magnetic fields are thrown into interplanetary space (Kahler, 1987). The total energy of a CME is similar to that of a large flare, that is, 10^{32} erg (Wagner, 1984). CMEs are usually associated with a prominence eruption or flares (Compagnino et al., 2017). When CMEs are directed toward Earth, they are called halo CMEs (Gopalswamy et al., 2010), due to a bright ring around the occulting disk of the coronograph. Halo CMEs are the most effective in generating geomagnetic storms (Lee et al., 2014) and causing damages to our technology such as satellites, power lines, GPS system, among others.

In this review, we will focus on the radio emission of the Sun from (1) the Quiet Sun emission following the solar cycle of 11 years, (2) active regions which vary according to the lifetime of sunspots (days to weeks), and (3) the sudden energetic flares that last from seconds to about an hour. The solar radio emission is detailed in the next section. More specifically, the goal of this review is on the main discoveries made with two Brazilian radio telescopes installed at the *Complejo Astronómico El Leoncito* (CASLEO) in Argentina that are described in the succeeding section. The main results from the observations of these telescopes are reported in the section that follows, whereas the conclusions are listed in the final section.

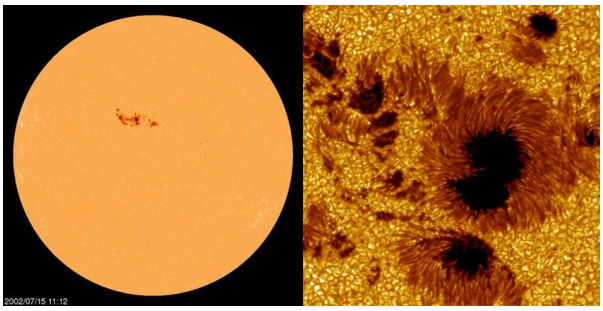

Figure 1: Images of the Sun on July 15th, 2002. Left: Image taken by MDI on board the SOHO (Solar and Heliospheric Observatory) spacecraft, at optical wavelengths (centered on the Ni I photospheric absorption line at 6767.8 Å). Right: Blowup of NOAA AR 10030 (dominant in the solar disk shown in the left panel) observed by the Swedish Solar Telescope, also at optical wavelengths.

SOLAR RADIO EMISSION

The Sun emits radiation throughout the whole electromagnetic spectrum, from the short wavelength X-rays to the radio long wavelengths, with the peak of the quiet Sun emission in the visible portion. The solar radio emission spans about 7 orders of magnitudes in frequency, from kHz to THz. The telescopes described here detect the high frequency emission of the Sun, from 45 to 405 GHz. Thus, here we concentrate on this frequency band. For a review of the radio emission on a broader spectra see Kundu (1965); Krüger (1979); Raulin and Pacini (2005); Bougeret and Pick (2007), and references therein.

Quiet Sun

Most of the long wavelength radio emission from the Sun originates from the corona, whereas the shorter wavelength radio waves arise generally from the lower chromosphere. The quiet solar radiation at radio wavelengths is produced by thermal free-free emission (Dulk, 1985) in the solar atmosphere. The height of the atmosphere where the emission of a certain frequency is produced can be determined from the radius measured in images of the Sun at that specific wavelength. Nevertheless, the uncertainty in the measurements at radio wavelengths is affected by the limb brightening (Selhorst et al., 2004) at these frequencies and also by the beam width of the instrument. Moreover, the method used for the radius calculation will also affect the results (Menezes et al., 2022).

Previous measurements of the solar radius from microwaves to submillimeter wavelengths are shown in Figure 2. The results in the figure clearly show that the radius of the solar limb, or the height above the photosphere where the emission is mostly produced, decreases as the frequency increases. This means that the higher frequency radio emission is produced at low heights in the solar atmosphere as compared to lower frequencies.

Active regions

The quiescent solar emission is produced at or above active regions. At radio wavelengths, active regions are usually bright (see Fig. 6) instead of the dark patches seen in white light images of the solar disk (Fig. 1). However, high resolution images of active regions observed by ALMA have shown the penumbra of sunspot to be dark at 230 GHz but not at 100 GHz (Loukitcheva et al., 2017). Nevertheless, Selhorst et al. (2014) reported that some active regions in radio were not associated to sunspots.

By detecting the emission of active regions at different radio wavelengths, the mechanism producing the radio emission can be determined. Moreover, the temperature, density, and even the magnetic field of the source of emission can be estimated. The emission mechanism responsible for the radio emission from active regions depends on the frequency (Dulk, 1985). Microwave emission, such as that observed by the Nobeyama Radio Heliograph (NoRH) at 17GHz, is known to be dueto gyroresonance from the thermal electrons gyrating around the magnetic field lines (Selhorst et al., 2008). On the other hand, high frequency emission (≥ 200 GHz) is believed to be due to free-free emission from thermal electrons, or thermal bremsstrahlung.

Flares

The transient radio emission is characteristic of solar activity such as flares. Chiefly, the radiation is produced throughout the whole electromagnetic spectrum, from the longest km waves all the way to the very short wavelength gamma-rays, by the energetic particles accelerated during the sudden energy release due to magnetic reconnection. Energetic electrons gyrating around the magnetic field lines emit microwaves by the gyrosynchrotron mechanisms, whereas coherent plasma emission produces the lower frequency (< 1GHz) radio emission (Dulk, 1985; McLean and Labrum, 1985).

The temporal evolution of a solar flare can be divided into three main phases: the preflare, the impulsive, and the decay pha- ses (Benz, 2008). The flare evolution at different wavelength is shown in Figure 3. Depending on the emission mechanisms at work during each phase, different electromagnetic radiation dominates. During the impulsive phase, the accelerated electrons produce high frequency radio emission (such as microwaves, millimeter, and submillimeter) as they gyrate around magnetic field lines. These same electrons will also produce hard X-rays as they precipitate into the chromosphere and interact with the ions of the atmosphere (Benz, 2017; Cliver et al., 2022). On the other hand, as particles thermalize and the plasma is heated, soft-X rays are produced.

Since the temporal evolution of the radio emission during solar flares is very similar to that of the X-rays (see Fig. 3), it is believed that both emissions are produced by a common population of accelerated electrons (White et al., 2011). In this scenario, nonthermal electrons emit X-rays due to bremsstrahlung once they collide with the denser lower chromosphere. On the other hand, accelerated electrons from the same population produce radio emission by different mechanisms depending on the frequency: microwaves originate from gyrosynchrotron, whereas millimetric and submillimetric wavelength emissions arise from a combination of gyrosynchrotron (during the impulsive phase) and thermal bremsstrahlung (during the decay phase) (Dulk, 1985).

THE RADIO TELESCOPES: POEMAS AND SST

Two Brazilian radio telescopes, located at CASLEO in Argentina, have been monitoring the Sun daily. The solar dedicated radio antennae are the POlarization Emission of Millimeter Solar Activity (POEMAS), a system of two polarimeters operating at the frequencies of 45 and 90 GHz, and the Solar Submillimeter Telescope (SST) that observes the Sun at 212 and 405 GHz. SST has been monitoring the Sun since 1999, for over two activity cycles.

POEMAS telescope - 45 and 90 GHz

The POEMAS consists of two telescopes that measure right- and left-hand circular polarizations of solar emission at 45 and 90 GHz (Valio et al., 2013). Installed at CASLEO, the telescope shown in Figure 4

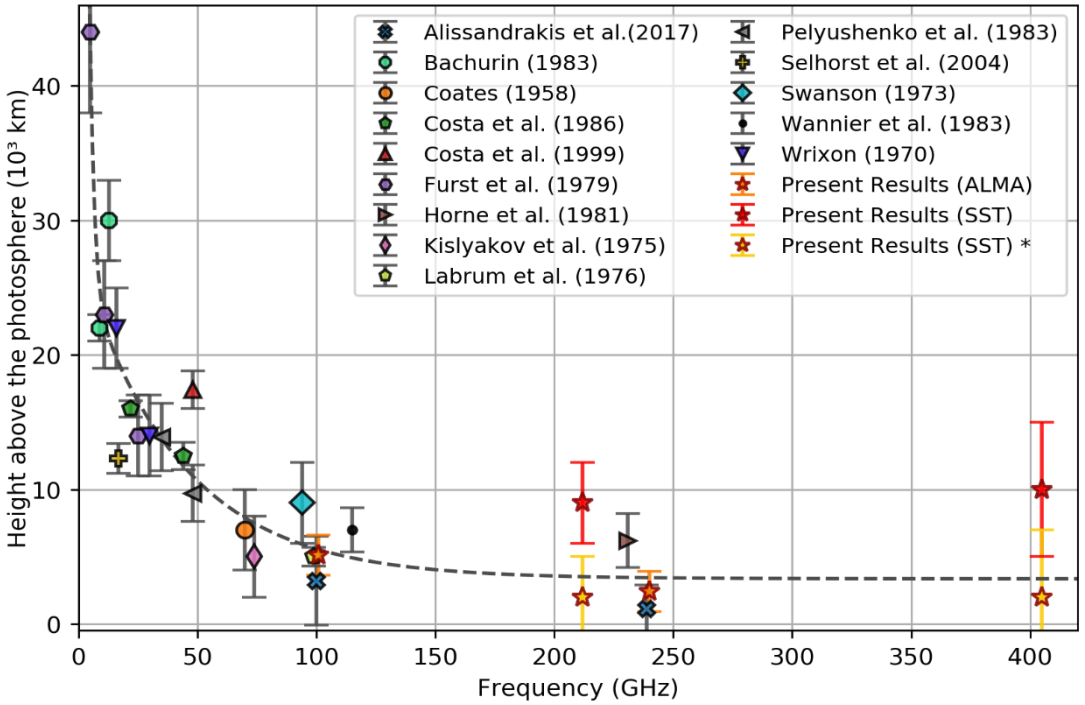

Figure 2: Height above the photosphere of the radio solar emission as a function of the frequency, from 1 to 400 GHz. The points identified as "Present results (SST)" are previous SST results from Menezes et al. (2021), whereas the updated values using the inflection point method reported in Menezes et al. (2022) are marked as "Present results (SST)*". Data of solar limb measurements at other radio frequencies were collected from several works (Coates et al., 1958; Wrixon, 1970; Swanson, 1973; Kislyakov et al., 1975; Labrum et al., 1978; Fuerst et al., 1979; Horne et al., 1981; Bachurin, 1983; Pelyushenko and Chernyshev, 1983; Wannier et al., 1983; Costa et al., 1986, 1999; Selhorst et al., 2004; Alissandrakis et al., 2017).

observes the full disk of the Sun with a time resolution of 10 ms at both frequencies, and a sensitivity of 2 – 4 K which corresponds to 4 and 20 solar flux unit (1 SFU = 10^4 Jy). The telescope was installed in November 2011 and operated successfully until December 2013. During this period POEMAS detected over 30 solar flares from 2012 through 2013 (Hidalgo Ramírez et al., 2019).

Solar Submillimeter Telescope - 212 and 405 GHz

Since 1999, the SST has been monitoring the Sun from the CASLEO Observatory (Kaufmann et al., 1997). It consists of a 1.5m antenna with 6 total-power heterodyne room temperature receivers, four at 212 GHz and two at 405 GHz. The half beam width of the antenna is nominally 4 arcmin at 212 GHz and 2 arcmin at 405 GHz. The temporal resolution of the observations is 5ms. A photograph of the radome enclosed telescope is shown on the left panel of Figure 5. A projection of the 6 beams of the telescope onto the yellow solar disk is shown in the left panel of Figure 5.

Because the beam of the SST telescope at both frequencies (212 and 405 GHz) is smaller than the solar disk, to produce an image of the Sun, also called a map, the telescope has to scan the solar disk (see right panel of Fig. 5). This mosaic of observations is then put together to produce the images shown in the top panels of Figure 6. As can be seen from the maps, active regions are seen as slightly brighter regions both at 212 and 405 GHz. At least 3 maps are produced daily from SST data, resulting in several thousand maps for the more than two decades of operation.

Both telescopes, POEMAS and SST, detected flares with high temporal resolution of less than 100ms. An interesting feature of flare emission at these high radio frequencies is that both the impulsive and the gradual phases are observed. From these observations new discoveries were made, which are described in the next section.

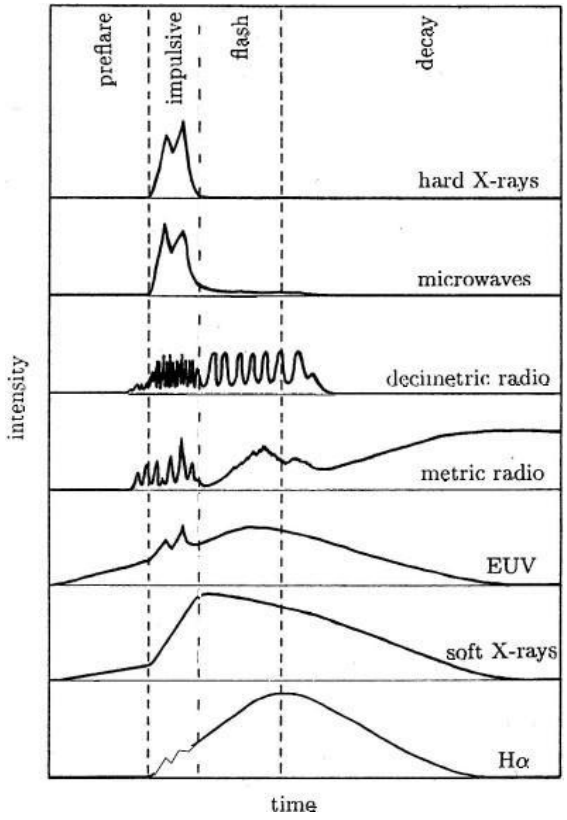

Figure 3: Temporal profile of the flare emission throughout the electromagnetic spectrum. There are basically three phases for the flare time evolution: preflare, impulsive, and decay (from Benz, 2008).

Figure 4: The POEMAS telescope at CASLEO Observatory in Argentina. The 44cm diameter antenna for the 45 GHz receiver is seen on the right of the image, whereas the 90 GHz telescope utilizes a 16.5 cm diameter lens, seen on the left (from Hidalgo Ramírez et al., 2019).

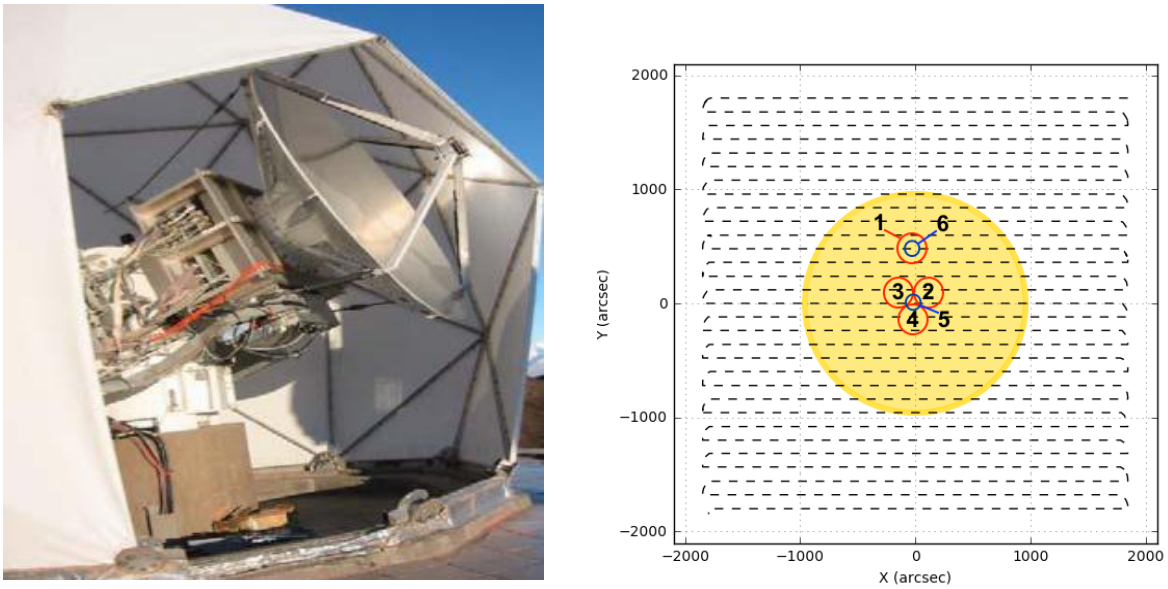

Figure 5: **Left:** Image of the Solar Submillimeter Telescope during installation. **Right:** Schematics of the Sun (yellow circle) with the projection of the four 212 GHz receivers (red circles) and the two 405 GHz receivers (blue circles). The dashed lines represent the path of the telescope while making a raster scan of the solar disk to produce a map of the Sun at submillimeter wavelengths

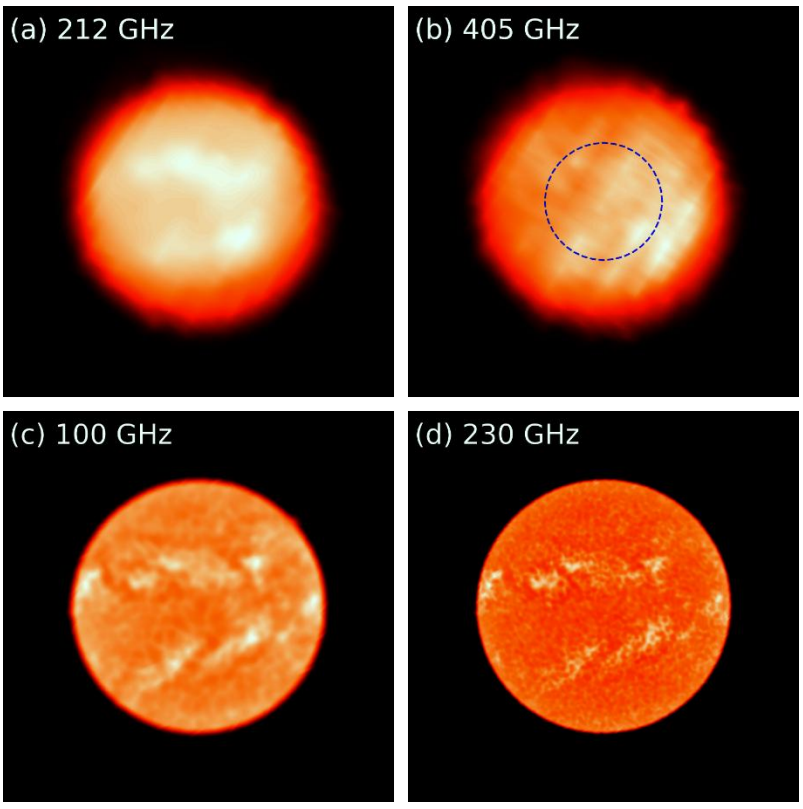

Figure 6: Maps of the Sun on December 17th, 2015. The top row is from SST at 212 (a) and 405 GHz (b). Bottom row maps were obtained from ALMA observations at 100 (c) and 230 GHz (d) (from Menezes et al., 2021).

SOLAR RADIUS, ACTIVE REGIONS, AND FLARES

Quiet Sun - solar radius

To determine at which height in the solar atmosphere the submillimeter emission is produced, the radius of the Sun is calculated. This is done by determining the limb of the Sun on the maps such as those shown in Figure 6. First, each raster scan of the Sun, or a row of the image (black line in Fig. 7a), is analyzed and the position of the limb is obtained from the inflection points (Thuillier et al., 2011). For that, the derivative of the scan profile (red curve in Fig. 7a) is calculated and the maximum and minimum points correspond to the inflection points, or limb coordinates. Next, all the limb points are then fit by a circumference (see Fig. 7b).

Menezes et al. (2021) analyzed over two decades of data from SST solar maps. Unfortunately, the first years had calibration problems and were discarded. Nevertheless, about 13 years of data were available for radius determination from SST maps. These results were further refined by Menezes et al. (2022) yielding measured average solar radius values of 963" ± 3" (212 GHz) and 963" ± 5" (405 GHz), indicated in Figure 2 as "Present Results (SST)*". The measured average radius at 212 GHz agrees very well with that obtained from the degraded ALMA maps at 230 GHz (Menezes et al., 2022). These average radii correspond to heights ≤ 3000km above the photosphere, that is, the quiet submillimter emission most likely originates from the lower chromosphere. Menezes et al. (2022) also estimated the limb brightening at submillimeter wavelengths by using forward modeling that resulted in 2 %-12 % at 212 GHz and 3 %-17 % at 405GHz.

Moreover, the variation of the solar radius in time along many years may reflect changes in the solar atmosphere related to the solar cycle. Therefore, crucial for the calibration of atmospheric models, the solar radius provides a better understanding of the solar atmospheric structure. Measurements of the solar radii at 212 and 405 GHz throughout many years (Menezes et al., 2022) are shown in the left and right panels of Figure 8, respectively. The temporal evolution of the SST radii over 13 years (2007 - 2019) is seen to be correlated to solar activity proxies such as the 10.7 flux or the mean magnetic field when considering equatorial regions of the solar atmosphere. On the other hand, an anticorrelation with the activity proxies is observed when considering the solar radius measured at polar regions. Since the submillimeter frequencies (212 and 405 GHz) are produced low in the solar atmosphere, these results may reflect the behavior from both the photosphere and the lower chromosphere. Perhaps this would explain the weak (212 GHz) and the moderate (405 GHz) correlation of the radii with the solar activity proxies.

Quiescent Sun - active regions

To determine the emission mechanism, the flux density spectra of the radio emission from active regions have to be construc- ted. Therefore, observations at different frequencies are needed. To characterize the radio source of active regions, Silva et al. (2005) studied 23 active regions observed in SST maps during the period of June/July of 2002. Maps at 212 and 405 GHz, such as those shown in the upper panel of Figure 6, were used in combination with maps of the Sun at 17 and 34 GHz from NoRH, where the brightest active region in the 212 GHz map was chosen for each day. The excess brightness temperature and their sizes were measured for each active region at the four frequencies. The quiet Sun level was estimated to be 5900K and 5100K at 212 and 405 GHz, respectively, from measurements of the new Moon at the same frequencies. A brightness excess in the range of 3 to 20 % was observed for the active regions, that is, 200-1000 K hotter, at both 212 and 405 GHz. The diameter of the submm source was estimated in the range of 2 - 7 arcmin and is approximately the same at both frequencies. The flux density spectra of all active regions, constructed from combining the submm and the microwave data, were seen to increase toward higher frequencies, with an average slope of 2. This slope is typical of free-free emission from thermal electrons in an optically thick source. Fits of the spectra by a thermal bremsstrahlung yield radio emitting sources with effective temperatures in the range of 6000 to 29000 K, and a lower limit to the density of 10^{10} cm^{-3}, assuming that the optical depth is unity at 405 GHz.

More recently, Valle Silva et al. (2021) analyzed active regions observed from 14 to 20 December 2015, a period of low solar activity. Besides maps from NoRH (17 GHz) and SST (212 and 405 GHz), the authors also considered Atacama Large Millimeter Array (ALMA) maps at 107 and 238 GHz. Spectra were constructed from the observations at these 5 frequencies and are shown in Figure 9. A linear fit was performed to the flux density spectra and again the spectral index is close to 2. These results are in agreement with those of previous works (Tsuchiya and Takahashi, 1968; Efanov et al., 1969; Kundu, 1970; Bastian et al., 1993; Tapping and Zwaan, 2001) and demonstrate that the emission from

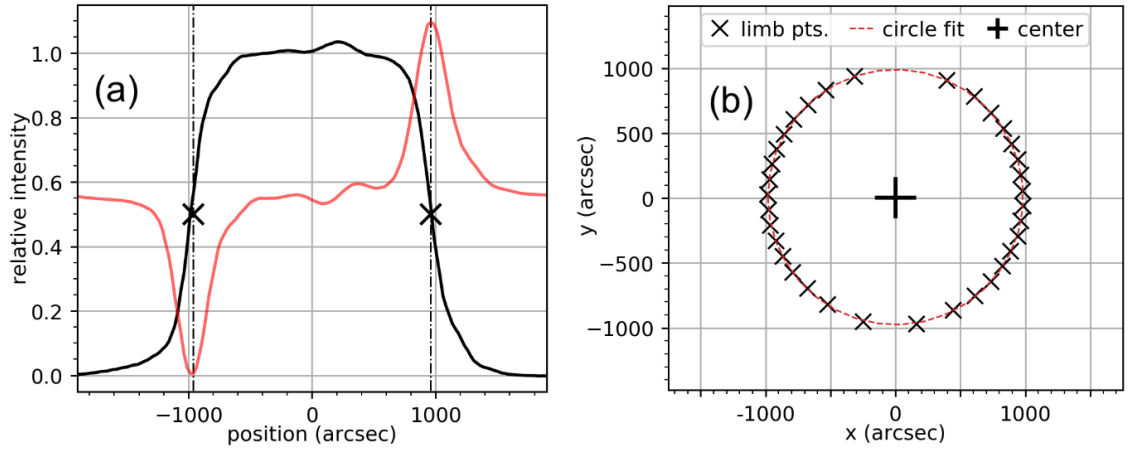

Figure 7: Estimate of the solar radius at submillimeter wavelengths. **(a)** Solar scan in black and its derivative in red. The inflection points of the scan are depicted by the crosses at the points of maximum and minimum inflection. **(b)** Limb points (crosses) fit by a circumference (red circle) (from Menezes et al., 2021).

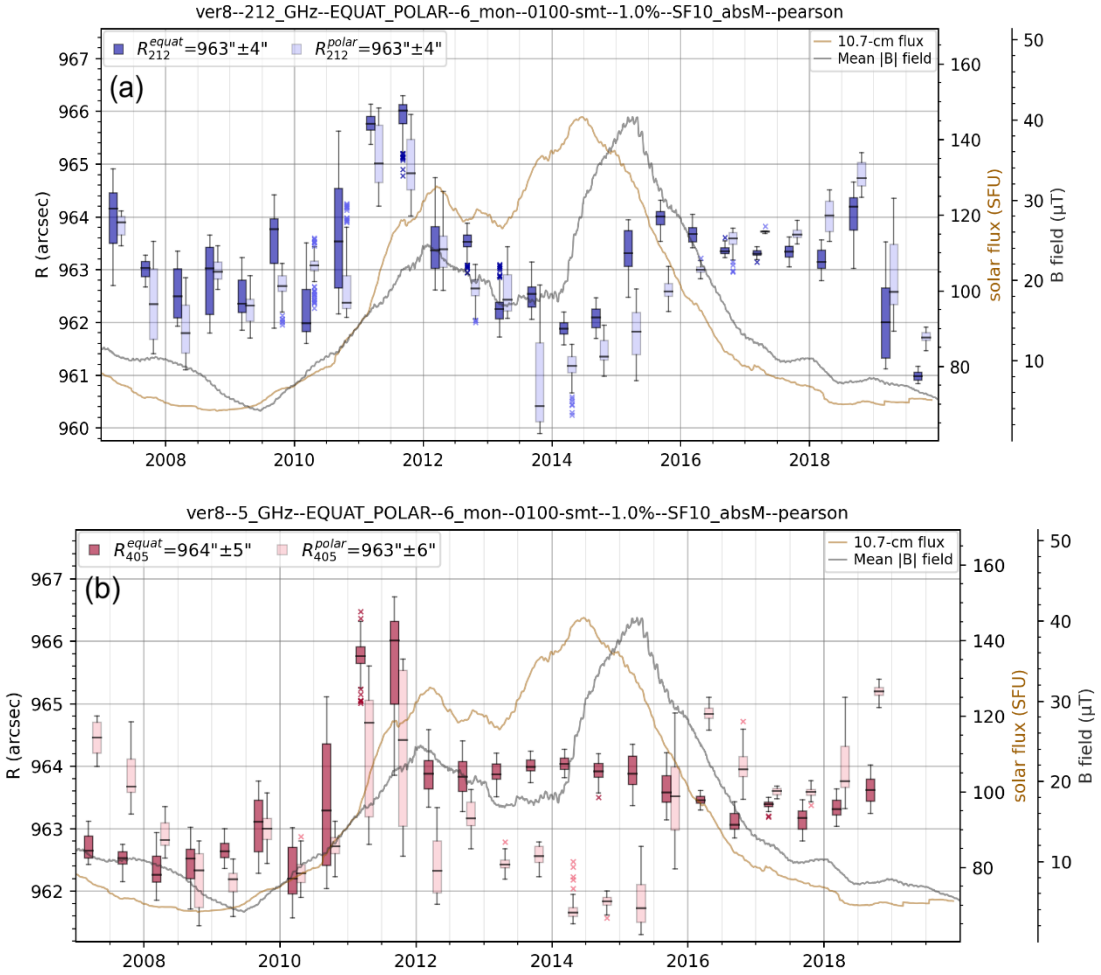

Figure 8: Solar radius at 212 and 405 GHz from January 2007 to December 2019. **(a)** Time series for equatorial (dark blue) and polar (light blue) radii at 212 GHz. **(b)** Time series for equatorial (red) and polar (pink) radii at 405 GHz. The orange and gray lines represent the 10.7cm flux and the mean magnetic field, respectively (from Menezes et al., 2021).

active regions at millimetric and submillimetric wavelengths is produced by thermal bremsstrahlung from sources located low in the chromosphere.

Active Sun - Flares

As mentioned earlier, a solar flare emits radiation throughout the entire electromagnetic spectrum. At radio wavelengths, the high frequency millimeter (45 and 90 GHz) and submillimeter (212 and 405 GHz) radiation may be due to gyrosynchrotron or thermal emission.

Silva and Valio (2021) studied in detail the solar flare that occurred on May 13th, 2013, observed by the POEMAS telescope at both 45 and 90 GHz and in hard X-rays above 1 MeV by RHESSI and Fermi space missions. The temporal profiles of the flare at both wavelengths were very similar, thus leading to believe that they originated from the same population of accelerated electrons. To determine if this was true, the radio spectrum and the hard X-ray spectrum were fit separately. From these fits, the electron energy distribution was determined. The result is shown in Figure 10 for three-time intervals during the flare.

The observed radio spectrum was fit by the Ramaty gyrosynchrotron emission model (Ramaty, 1969; Ramaty et al., 1994) and the optically thin radio spectral index was determined (red line of Fig. 10). Conversely, the hard X-ray spectral index was obtained by assuming thermal emission plus a nonthermal broken power-law distribution (black curve of Fig. 10). As can be seen from the electron energy distribution depicted on Figure 10, the index obtained from the radio spectrum agrees with the index of the X-ray spectrum for energies above a break energy of ~600 keV. Therefore, hard X-rays above 600 keV

and millimeter emission of solar flares are produced by the same population of high-energy accelerated electrons. This result implies that the energy distribution of accelerated electrons during large solar flares is best described by a broken power law, with a breakup above energies of 1 MeV.

Another interesting result from POEMAS is that of the polarized millimeter emission of the flares that occurred on February 17th, 2013 (Fig. 11) and November 5th, 2013. Polarization measurements at millimeter wavelengths of the two flares showed that the February 17th flare produced a smaller polarization degree, of only 5 %, in comparison to the 30 % degree of polarization of the November 5th, 2013 event (Silva et al., 2020). To determine the cause of this difference in polarization, we investigated the magnetic field configuration at the region of the two flares. For this analysis, we also combined data from 1-15 GHz of the Radio Solar Telescope Network (RSTN) and 212 GHz from SST. Both flares were also observed in hard X-rays by the RHESSI satellite. To determine the magnetic configuration at the flaring source, a model that simulates gyrosynchrotron emission in a spatially-varying 3D magnetic field loop structure was applied (Simões and Costa, 2006). In this model, the magnetic loop geometry is fixed and the field strength is the only free parameter of the magnetic field. Moreover, a uniform electron distribution was considered with two free parameters, the number density of energetic electrons and the electron spectral index.

Then, the flux and polarization radio spectra from 5 to 200 GHz of both flares were fit by this model. A good fit was obtained yielding the physical parameters of the loop and flaring sources. The best model fit to the 45 GHz data is shown in Figure 12 for both flares. The main result of this study was that the degree of polarization of a flare at millimeter wavelengths is related to the degree of asymmetry of the magnetic loop. High degree of polarization in a solar flare can be explained by two sources located at the footpoints of highly asymmetric magnetic loops, whereas low polarization degrees arise from footpoint sources of symmetric magnetic loops.

Strong solar flares are known to be preferentially **observed if they are** located near the solar limb in hard X- and γ-rays (Vestrand et al., 1987). Searching for a center-to-limb variation at millimeter wavelengths, Hidalgo Ramírez et al. (2019) analyzed a total of 30 flares detected by POEMAS at 45 GHz in both senses of polarization during a period of maximum solar activity. About half of these events were also detected at 90 GHz. The location of these 30 flares for three ranges of the 45 GHz flux density (<500 sfu, 500 − 1000 sfu, and >1000 sfu) is shown in Figure 13. From the results plotted in this figure, it is possible to see a slight correlation between the flux density of the flares and their heliocentric angle, implying that solar bursts with higher flux density have a higher probability to be located closer to the solar limb.

From this same data set, Hidalgo Ramírez et al. (2019) reported the reversal of the polarization sense for sources from east to west and from north to south, with few exceptions. Moreover, the degree of polarization at 45 GHz was larger than at 90 GHz for most of the events. These results are consistent with the sense of polarization given by the gyrosynchrotron emission model at high frequencies. According to the model, the degree of circular polarization in solar flares reflects the

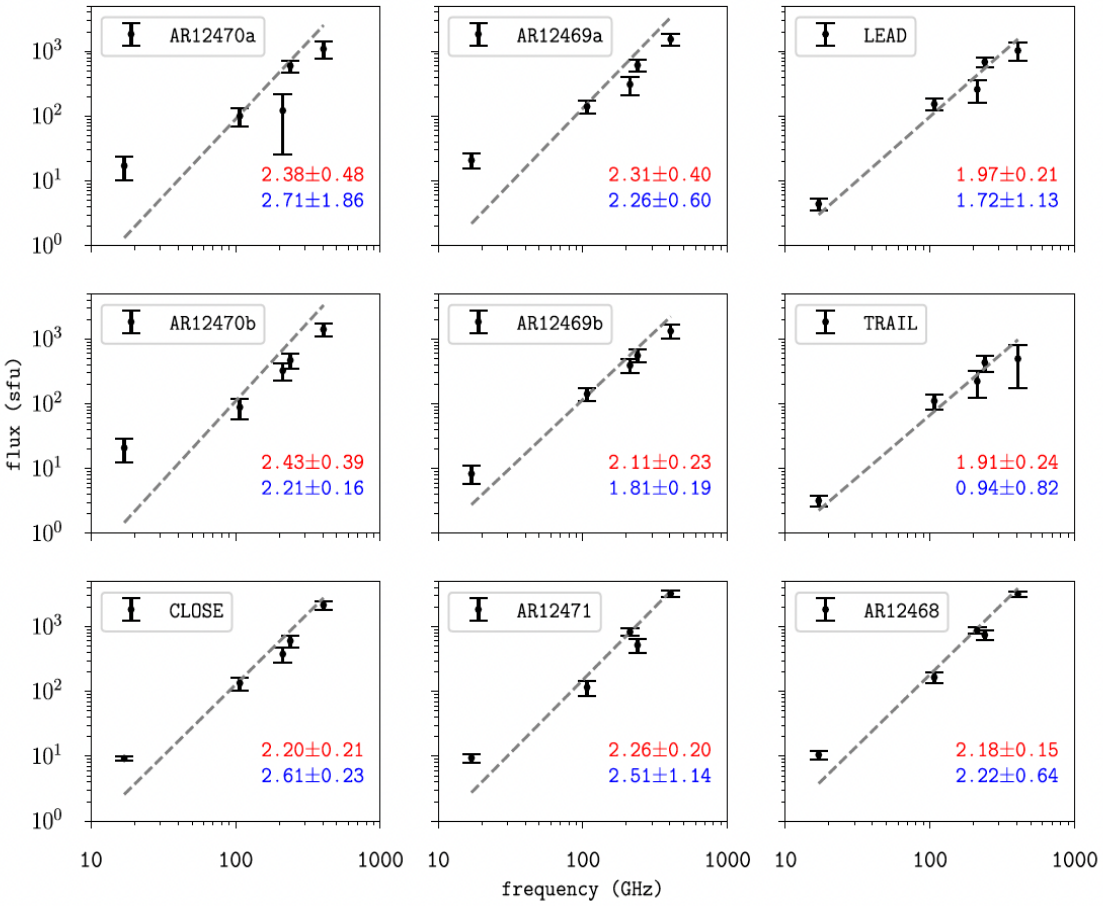

Figure 9: Density flux spectra of active regions. The spectral indexes fit to the spectra are given in each panel for frequencies between 17 and 405 GHz (red) and for frequencies above 100 GHz (blue) (from Valle Silva et al., 2021).

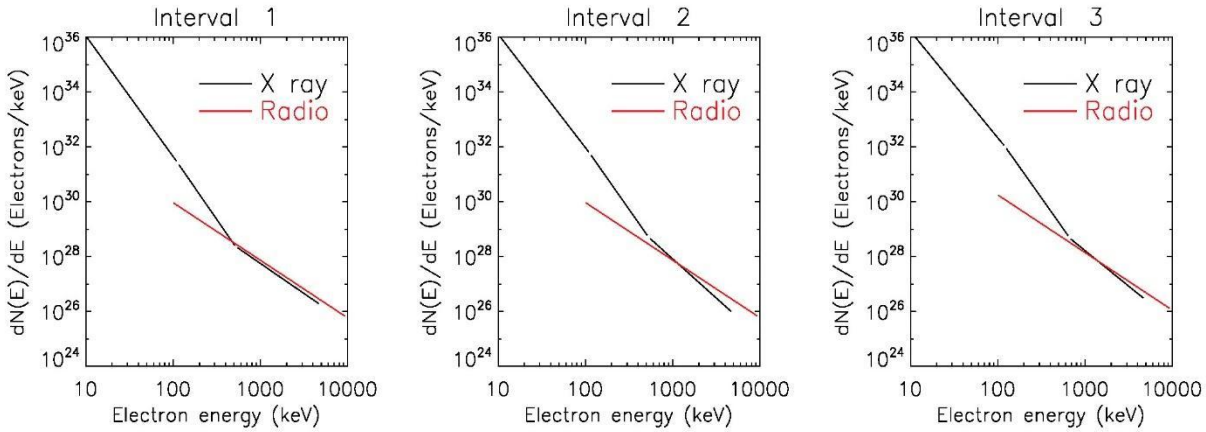

Figure 10: Broken power-law spectrum of the accelerated electron energy distribution for three-time intervals during the flare. The black curve was extracted from the hard X-ray data, whereas the red line, from the radio emission (from Silva and Valio, 2021).

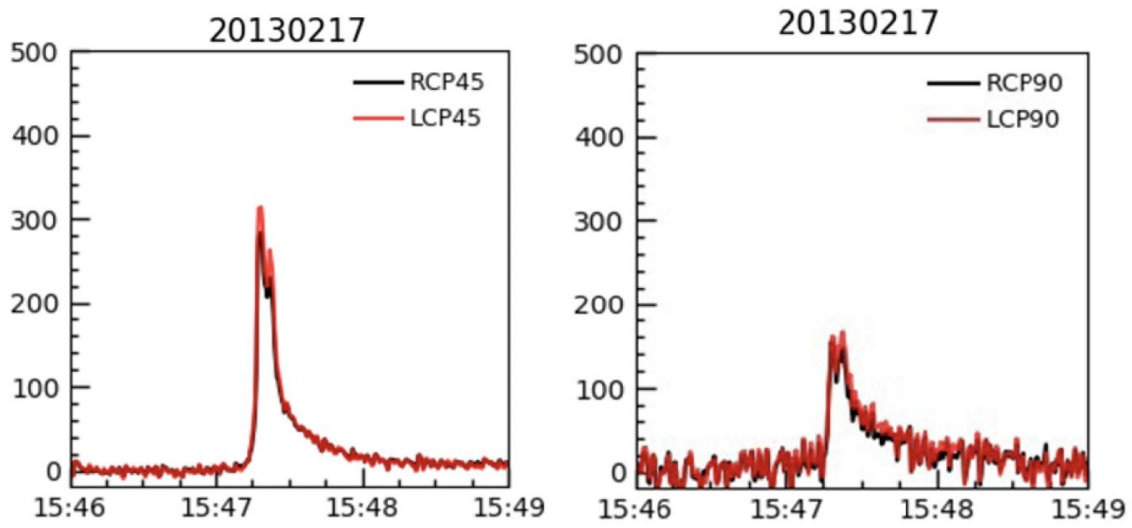

Figure 11: Millimeter light curve of the flare that occurred on February 17th, 2013, at around 15:47:22 UT. The right- (RCP in black) and left-hand (LCP in red) circular polarization emissions at 45 GHz and 90 GHz are shown in the left and right panels, respectively. Extracted from Hidalgo Ramírez et al. (2019).

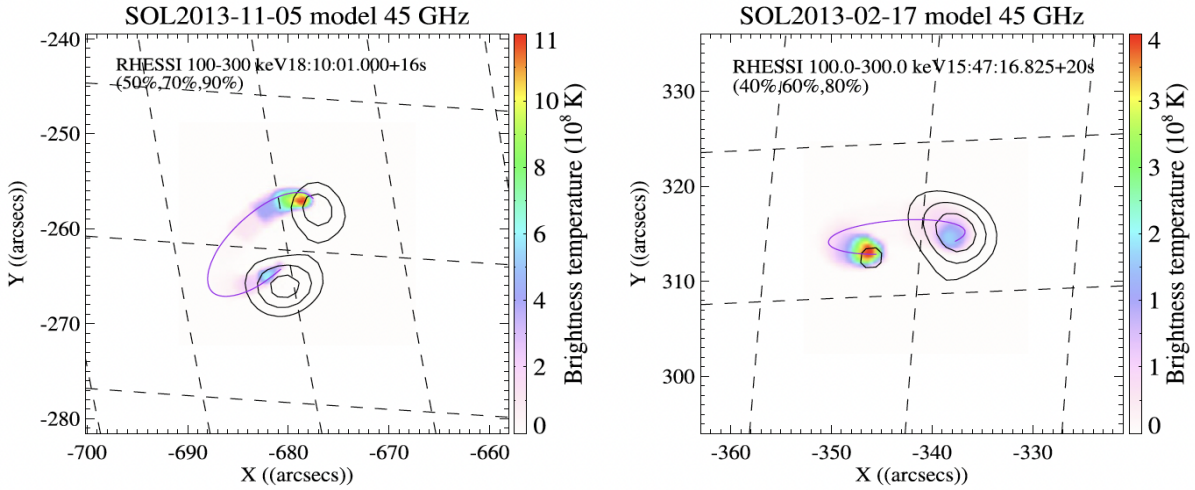

Figure 12: Maps of 45 GHz brightness temperature from the model calculations for February 17th (right) and November 5th, 2013 (left) solar flares. RHESSI HXR contours are shown for reference. The magnetic loop geometry resulting from the model is depicted by the purple line (from Silva et al., 2020).

dominant magnetic polarity of the flaring region instead of the large scale magnetic loop of the active region (Tanaka and Kakinuma, 1959).

Finally, probably the most important result from observations of the Solar Submillimeter Telescope is the detection of a new spectral component that increases toward higher frequencies, contrary to what was expected. Because there was a lack of flare observations at frequencies higher than 100 GHz, this spectral component went unnoticed. Kaufmann et al. (2004) reported on the submm observations of the November 4th, 2003, the largest flare ever detected, X28 according to GOES classification. This event was also observed by the Owens Valley Solar Array (OVSA) at microwaves from 1.2 to 18 GHz and also at 44 GHz by the Itapetinga Observatory (today renamed to Pierre Kaufmann Radio Observatory). Light curves of the submm emission and that of the 15.6 GHz are shown in the left panel of Figure 14. Spectra were collected at the time intervals marked in this panel that combined microwave and submm data. The spectra at time intervals P1 and P4 are shown in the right panel of Figure 14. As can be seen from the figure, the two submm flux densities at 212 and 405 GHz

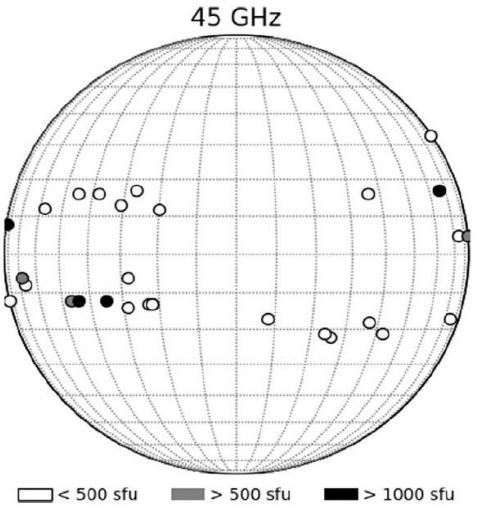

Figure 13: Distribution of the heliographic coordinates and intensity of solar bursts at 45 GHz observed by POEMAS. White circles represent peak flux <500 sfu, gray circles represent peak flux in the range of 500-1000 sfu, and black circles represent peak flux >1000 sfu (from Hidalgo Ramírez et al., 2019).

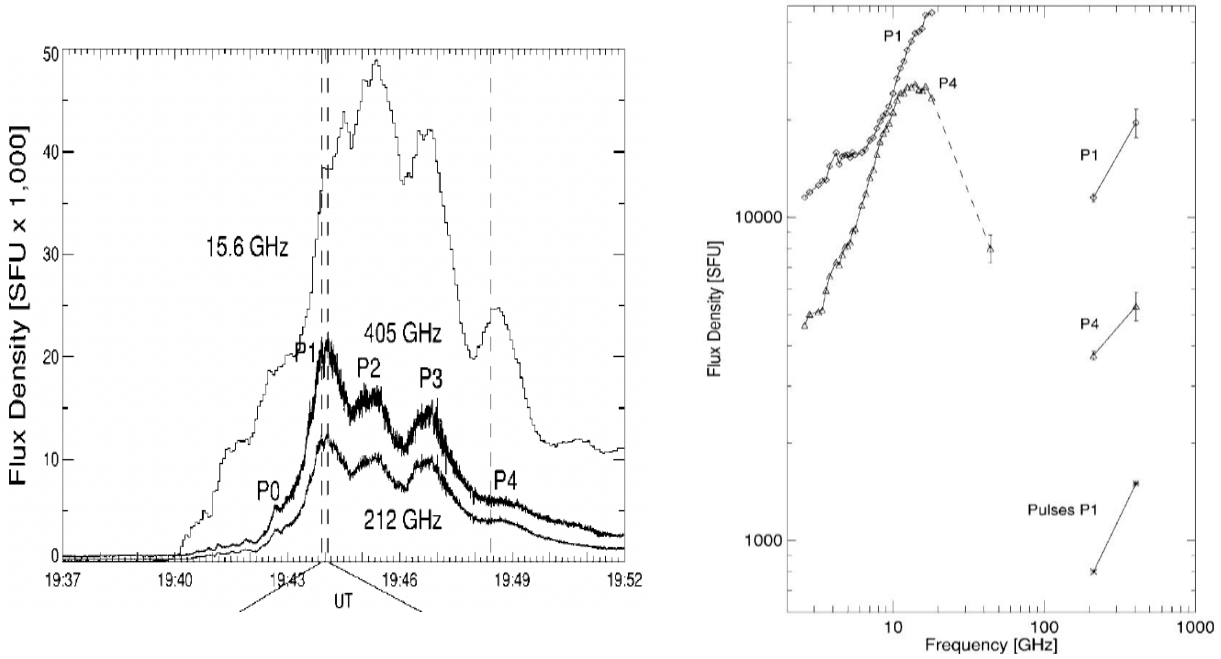

Figure 14: **Left:** Light curve of the burst at 405, 212, and 15.6 GHz in units of 10^3 sfu. The temporal resolution is 40 ms for the submillimeter data, while that of OVSA data is 4 s. **Right:** Spectra of the burst exhibiting two distinct components for the major peak P1 (diamonds) and for the smaller peak P4 (triangles). The spectra consist of OVSA 1.2–18 GHz microwave data and SST 212 and 405 GHz. During peak P4, there were 44 GHz data obtained by Itapetinga (from Kaufmann et al., 2004).

do not fall into the decreasing prolongation of the microwave spectrum, but rather indicate a new rising spectral component, which should peak somewhere in the THz frequency domain.

The origin of this new spectral THz component is still unknown. One possible explanation is that this component arises from a small source located near the magnetic loop footpoint, deep within the solar chromosphere. This source is different from the source emitting in microwaves which would be somewhere in the magnetic loop top. This double source scenario was able to explain the radio emission of yet another large solar flare detected at submm, microwaves, hard- and γ-rays (Silva et al., 2007). Another possible cause is based on laboratory accelerator experiments, where perturbations produce electron beam density

modulations, called microbunching (Klopf et al., 2014). These instabilities produce broadband coherent synchrotron emission at wavelengths similar to the size of the microbunch. This coherent synchrotron radiation is much stronger and peaks at larger frequencies than the “normal" microwave component. Other solar flares have been observed at submm wavelengths, but not all present this increasing spectral component (Raulin et al., 2004; Cristiani et al., 2005; Giménez de Castro et al., 2009, 2013; Trottet et al., 2011; Raulin et al., 2014).

CONCLUSIONS

Highlights of recent observations from two solar dedicated radio telescopes (SST and POEMAS) have been presented. These were mainly the results from the analysis of maps of the quiet Sun, spectra of active regions, and multiwave- length studies of solar flares. Measurements of the solar radius from solar maps determine approximately the height in the atmosphere where the radio emission originates. The emission at frequencies of 212 and 405 GHz arises from approximately 3", or ≤ 3000 km above the photosphere (Menezes et al., 2022). The solar submm radius is also seen to vary with the 11-year Solar Activity Cycle.

Active regions were seen as bright areas on solar submm radio maps. From the modeling of their combined radio spectra, the emission of active regions at high frequencies (>17 GHz) was determined to be due to optically thick thermal bremsstrahlung radiation.

Solar flares observed at millimeter wavelengths exhibited a broken power-law spectra of the energy distribution of nonthermal electrons, in accordance with the hard X-ray observations, implying thus that both the millimeter and the hard X-rays are produced by the same population of accelerated electrons. The degree of polarization observed for some flares seems to be related to the asymmetry of the magnetic loop where the flare occurred. Symmetric loops produce flares with lower polarization degree, whereas highly asymmetric loops produce higher polarization. A slight directivity of the flare emission at millimeter wavelengths was also found, where more intense burst had a tendency to be located closer to the solar limb.

Finally, a new spectral component of radio emission at very high frequencies (THz) was discovered from the observation of the largest solar flare detected to date, which occurred on November 4, 2003. The flux density spectrum at submm wavelengths increased toward higher frequencies showing it not to be a mere prolongation of the known microwave component generally attributed to gyrosynchrotron mechanism. Further observations at even higher frequencies (for example, in the far infrared) are **needed** to shed light onto this new phenomenon.

ACKNOWLEDGEMENTS

The authors would like to thank the insightful suggestions of the referees which much improvedthis article.

REFERENCES

Alissandrakis, C. E., S. Patsourakos, A. Nindos, and T. S. Bastian, 2017, Center-to-limb observations of the Sun with ALMA. Implications for solar atmospheric models: Astronomy & Astrophysics, **605**, A78, doi: 10.1051/0004-6361/201730953.

Bachurin, A. F., 1983, Variation in solar radio radius with the phase of the solar activity cycle at wavelengths of 2.25 and 3.5 CM: Izvestiya Ordena Trudovogo Krasnogo Znameni Krymskoj Astrofizicheskoj Observatorii, **68**, 68–75.

Bastian, T. S., M. W. Jr. Ewell, and H. Zirin, 1993, The Center-to-Limb Brightness Variation of the Sun at lambda = 850 Microns: The Astrophysical Journal, **415**, 364, doi: 10.1086/173170.

Benz, A. O., 2008, Flare Observations: Living Reviews in Solar Physics, **5**, 1, 1, doi: 10.12942/lrsp-2008-1.

Benz, A. O., 2017, Flare Observations: Living Reviews in Solar Physics, **14**, 1, 2, doi: 10.1007/s41116-016-0004-3.

Bougeret, J.-L., and M. Pick, 2007, Solar Radio Emissions, *in* Kamide, Y., and A. Chian, Eds., Handbook of the Solar-Terrestrial Environment: Springer-Verlag Berlin Heidelberg. p. 133–151.

Cliver, E. W., C. J. Schrijver, K. Shibata, and I. G. Usoskin, 2022, Extreme solar events: Living Reviews in Solar Physics, **19**, 1, 2, doi: 10.1007/s41116-022-00033-8.

Coates, R. J., J. E. Gibson, and J. P. Hagen, 1958, The 1954 Eclipse Measurement of the 8.6-MM Solar Brightness Distribution: The Astrophysical Journal, **128**, 406, doi: 10.1086/146554.

Compagnino, A., P. Romano, and F. Zuccarello, 2017, A Statistical Study of CME Properties and of the Correlation between Flares and CMEs over Solar Cycles 23 and 24: Solar Physics, **292**, 5, doi: 10.1007/s11207-016-1029-4.

Costa, J. E. R., J. L. Homor, and P. Kaufmann, 1986, Single-dish high sensitivity determination of solar limb emission at 22 and 44 GHz, *in* Tandberg, E., R. M. Wilson, and R. M. Hudson, Eds., Solar Flares and Coronal Physics Using P/OF as a Research Tool: NASA Conference Publication, Alabama, 2421, p. 201–207.

Costa, J. E. R., A. V. R. Silva, V. S., Makhmutov, E. Rolli, P. Kaufmann, and A. Magun, 1999, Solar Radius Variations at 48 GHZ correlated with Solar Irradiance: The Astrophysical Journal, **520**, 1, L63–L66, doi: 10.1086/312132.

Cristiani, G., G. Martínez, C. H. Mandrini, C. G. G. De Castro, M. G. Rovira, P. Kaufmann, and H. Levato, 2005, Submillimeter-wave and H α observations of the event on 28 November, 2001: Journal of Atmospheric and Solar-Terrestrial Physics, **67**, 1744–1750, doi: 10.1016/j.jastp.2005.02.025.

Dulk, G. A., 1985, Radio emission from the sun and stars: Annual Review of Astronomy and Astrophysics, **23**, 169–224, doi: 10.1146/annurev.aa.23.090185.001125.

Efanov, V. A., A. G. Kislyakov, I. G. Moiseev, and A. I. Naumov, 1969, Observation of Solar Radio Emission by the 22-m Radio Telescope at the Crimean Astrophysical Observatory at 2.25 mm and 8.15 mm Wavelengths. Solar Physics, **8**, 2, 331–340, doi: 10.1007/BF00155380.

Emslie, A. G., H. Kucharek, B. R. Dennis, N. Gopalswamy, G. D. Holman, G. H. Share, A. Vourlidas, T. G. Forbes, P. T. Gallagher, G. M. Mason, T. R. Metcalf, R. A. Mewaldt, R. J. Murphy, R. A. Schwartz, and T. H. Zurbuchen, 2004, Energy partition in two solar flare/CME events: Journal of Geophysical Research (Space Physics), **109**, A10, A10104, doi: 10.1029/2004JA010571.

Fuerst, E., W. Hirth, and P. Lantos, 1979, The radius of the sun at centimeter waves and the brightness distribution across the disk: Solar Physics, **63**, 2, 257–270, doi: 10.1007/BF00174532.

Giménez de Castro, C. G., G. D. Cristiani, P. J. A. Simões, C. H. Mandrini, E. Correia, and P. Kaufmann, 2013, A Burst with Double Radio Spectrum Observed up to 212 GHz: Solar Physics, **284**, 2, 541–558, doi: 10.1007/s11207-012-0173-8.

Giménez de Castro, C. G., G. Trottet, A. Silva-Valio, S. Krucker, J. E. R. Costa, P. Kaufmann, E. Correia, and H. Levato, 2009, Submillimeter and X-ray observations of an X class flare": Solar Physics, **507**, 1, 433–439, doi: 10.1051/0004-6361/200912028.

Gopalswamy, N., S. Yashiro, G. Michalek, H. Xie, P. Mäkelä, A. Vourlidas, and R. A. Howard, 2010, A Catalog of Halo Coronal Mass Ejections from SOHO: Sun and Geosphere, **5**, 1, 7–16.

Hathaway, D.H., 2015, The Solar Cycle. Living Reviews in Solar Physics, **12**, 4, doi: 10.1007/lrsp-2015-4.

Heyvaerts, J., E. R. Priest, and D. M. Rust, 1977, An emerging flux model for the solar phenomenon: The Astrophysical Journal, **216**, 123–137, doi: 10.1086/155453.

Hidalgo Ramírez, R. F., A. Morosi, D. Silva, P. J. A. Simos, and A. Valio, 2019, Center-to-Limb Variation of Solar Bursts Polarization at Millimeter Wavelengths: Solar Physics, **294**, 8, 108, doi: 10.1007/s11207-019-1503-x.

Horne, K., G. J. Hurford, H. Zirin, and T. De Graauw, 1981, Solar limb brightening at 1.3 millimeters. The Astrophysical Journal, 244, 340–344, doi: 10.1086/158711.

Hudson, H. S., and R. C. Willson, 1983, Upper Limits on the Total Radiant Energy of Solar Flares, *in* Kane, S.R., Y. Uchida, K. Tanaka, and H.S. Hudson, Eds., Recent Advances in the Understanding of Solar Flares: Solar Physics, Springer, Dordrecht, **86**, 1-2, 123–130, doi: 10.1007/978-94-009-7228-5_14.

Kahler, S., 1987, Coronal mass ejections: Reviews of Geophysics, **25**, 3, 663–675, doi: 10.1029/RG025i003p00663.

Kaufmann, P., J. E. R. Costa, E. Correia, A. Magun, K. Arzner, N. Kämpfer, M. Rovira, and H. Levato, 1997, Recent Developments of the Solar Submm-Wave Telescope (SST), *in* Trottet, G., Ed., Coronal Physics from Radio and Space Observations, **483**, p. 202, doi: 10.1007/BFb0106459.

Kaufmann, P., J. E. R. Costa, E. Correia, C. G. G. De Castro, J.-P. Raulin, and A. V. R. Silva, 2000, Multiple High Energy Injections at the Origin of Solar Flares, *in* Ramaty, R., and N. Mandzhavidze, Eds., High Energy Solar Physics Workshop - Anticipating HESSI, Astronomical Society of the Pacific Conference Series, **206**, p. 318.

Kaufmann, P., J.-P. Raulin, C. G. G. De Castro, H. Levato, D. E. Gary, J. E. R. Costa, A. Marun, P. Pereyra, A. V. R. Silva, and E. Correia, 2004, A New Solar Burst Spectral Component Emitting Only in the Terahertz Range: The Astrophysical Journal, **603**, 2, L121–L124, doi: 10.1086/383186.

Kerr, G. S., 2022, Interrogating solar flare loop models with IRIS observations 1: Overview of the models, and mass flows: Frontiers in Astronomy and Space Sciences, Frontiers Media SA., **9**, 1060856, doi: 10.3389/fspas.2022.1060856.

Kislyakov, A. G., I. I. Kulikov, L. I. Fedoseev, and V. I. Chernyshev, 1975, Observations of the sun at 1.4 and 4.1 MM wavelength with 13-arcsecond and 40-arcsecond resolution: Soviet Astronomy Letters, **1**, 79.

Klopf, J. M., P. Kaufmann, J.-P. Raulin, and S. Szpigel, 2014, The Contribution of Microbunching Instability to Solar Flare Emission in the GHz to THz Range of Frequencies: The Astrophysical Journal, **791**, 1, 31, doi: 10.1088/0004-637X/791/1/31.

Krüger, A., 1979, Introduction to solar radio astronomy and radio physics: Geophysics and Astrophysics Monographs, GAAM, **16**, 345 p., Dordrecht, D. Reidel Publishing Co., doi: 10.1007/978-94-009-9402-7.

Kundu, M. R., 1965, Solar radio astronomy: Interscience Publication, New York, 660 p.

Kundu, M. R., 1970, Solar Active Regions at Millimeter Wavelengths: Solar Physics, **13**, 2, 348–356, doi: 10.1007/BF00153556.

Labrum, N. R., J. W. Archer, and C. J. Smith, 1978, Solar brightness distribution at 3 mm wavelength from observations of the eclipse of 1976 October 23: Solar Physics, 59, 331–343, doi: 10.1007/BF00951837.

Lee, J.-O., Y. J. Moon, K.-S. Lee, and R. S. Kim, 2014, Dependence of Geomagnetic Storms on Their Associated Halo CME Parameters: Solar Physics, **289**, 6, 2233–2245, doi: 10.1007/s11207-013-0466-6.

Loukitcheva, M. A., K. Iwai, S. K. Solanki, S. M. White, and M. Shimojo, 2017, Solar ALMA Observations: Constraining the Chromosphere above Sunspots: The Astrophysical Journal, **850**,

1, 35, doi: 10.3847/1538-4357/aa91cc.

McLean, D. J., and N. R. Labrum, 1985, Solar radiophysics: studies of emission from the sun at metre wavelengths: Cambridge University Press, 540 pp.

Melrose, D. B., 1990, Particle acceleration processes in the solar corona: Australian Journal of Physics, **43**, 6, 703–752, doi: 10.1071/PH900703.

Menezes, F., C. L. Selhorst, C. G. G. De Castro, and A. Valio, 2021, The Subterahertz Solar Cycle: Polar and Equatorial Radii Derived from SST and ALMA: The Astrophysical Journal, **910**, 1, 77, doi: 10.3847/1538-4357/abe41c.

Menezes, F., C. L. Selhorst, C. G. Giménez de Castro, and A. Valio, 2022, Subterahertz radius and limb brightening of the Sun derived from SST and ALMA: Monthly Notices of the Royal Astronomical Society, **511**, 1, 877–885, doi: 10.1093/mnras/stab3501.

Pelyushenko, S. A., and V. I. Chernyshev, 1983, The Radio Radius of and Brightness Distribution Over the Solar Disk at Wavelengths of 6.3 and 8.6 mm: Soviet Astronomy, **27**, 340.

Ramaty, R., 1969, Gyrosynchrotron Emission and Absorption in a Magnetoactive Plasma: The Astrophysical Journal, **158**, 753, doi: 10.1086/150235.

Ramaty, R., R. A. Schwartz, S. Enome, and H. Nakajima, 1994, Gamma-Ray and Millimeter-Wave Emissions from the 1991 June X-Class Solar Flares: The Astrophysical Journal, **436**, 941–949, doi: 10.1086/174969.

Raulin, J. P., V. S. Makhmutov, P. Kaufmann, A. A. Pacini, T. Lüthi, H. S. Hudson, and D. E. Gary, 2004, Analysis of the impulsive phase of a solar flare at submillimeter wavelengths: Solar Physics, **223**, 1–2, 181–199, doi: 10.1007/s11207-004-1300-y.

Raulin, J.-P., and A. A. Pacini, 2005, Solar radio emissions, *in* Jatenco-Pereira, V., A. C.-L. Chian, J. F. Valdes-Galicia, M. A. Shea, Eds., Fundamentals of Space Environment Science: Advances in Space Research, **35**, 5, 739–754, doi: 10.1016/j.asr.2005.03.138.

Raulin, J.-P., G. Trottet, G. G. De Castro, T. Lüthi, and P. Kaufmann, 2014, Joint Measurements of Flare Flux Densities at 210 - 212 GHz by Two Different Radio Telescopes: Solar Physics, **289**, 4, 1227–1237, doi: 10.1007/s11207-013-0390-9.

Selhorst, C. L., J. E. R. Costa, C. G. Giménez de Castro, A. Valio, A. A. Pacini, and K. Shibasaki, 2014, The 17 GHz Active Region Number: The Astrophysical Journal, **790**, 2, 134, doi: 10.1088/0004-637X/790/2/134.

Selhorst, C. L., A. V. R. Silva, and J. E. R. Costa, 2004, Radius variations over a solar cycle: Astronomy and Astrophysics, **420**, 3, 1117–1121, doi: 10.1051/0004-6361:20034382.

Selhorst, C. L., A. Silva-Válio, and J. E. R. Costa, 2008, Solar atmospheric model over a highly polarized 17 GHz active region: Astronomy and Astrophysics, **488**, 3, 1079–1084, doi: 10.1051/0004-6361:20079217.

Silva, A. V. R., T. F. Laganá, C. G. G. de Castro, P. Kaufmann, J. E. R. Costa, H. Levato, and M. Rovira, 2005, Diffuse Component Spectra of Solar Active Regions at Submillimeter Wavelengths: Solar Physics, **227**, 2, 265–281, doi: 10.1007/s11207-005-2787-6.

Silva, A. V. R., G. H. Share, R. J. Murphy, J. E. R. Costa, C. G. G. De Castro, J. P. Raulin, and P. Kaufmann, 2007, Evidence that Synchrotron Emission from Nonthermal Electrons Produces the Increasing Submillimeter Spectral Component in Solar Flares: Solar Physics, **245**, 2, 311–326, doi: 10.1007/s11207-007-9044-0.

Silva, D. F., P. J. A. Simões, R. F. Hidalgo Ramírez, and A. Válio, 2020, Inferring the Magnetic Field Asymmetry of Solar Flares from the Degree of Polarisation at Millimetre Wavelengths: Solar Physics, **295**, 6, 73, doi: 10.1007/s11207-020-01632-0.

Silva, D. F., and A. Valio, 2021, Broken Power-law Energy Spectra of the Accelerated Electrons Detected in Radio and Hard X-Rays during the SOL2013-05-13 Event: The Astrophysical Journal, **915**, 1, L1, doi: 10.3847/2041-8213/ac0726.

Simões, P. J. A., and J. E. R. Costa, 2006, Solar bursts gyrosynchrotron emission from three-dimensional sources: Astronomy and Astrophysics, **453**, 2, 729–736, doi: 10.1051/0004-6361:20054665.

Swanson, P. N., 1973, The Radio Radius of the Sun at Millimeter and Centimeter Wavelengths: Solar Physics, **32**, 77–80, doi: 10.1007/BF00152730.

Takeda, A., L. Acton, and N. Albanese, 2019, Solar Cycle Variation of Coronal Temperature, Emission Measure, and Soft X-Ray Irradiance Observed with Yohkoh Soft X-Ray Telescope: The Astrophysical Journal, **887**, 2, 225, doi: 10.3847/1538-4357/ab53e3.

Tanaka, H., and T. Kakinuma, 1959, Polarization of bursts of solar radio emission at microwave frequencies, *in* Bracewell, R. N., Ed., Paris Symposium on Radio Astronomy, International Astronomical Union, International Scientific Radio Union, USRI, Stanford University Press, **9**, 215–217, doi: 10.1017/S0074180900050877.

Tapping, K. F., and C. Zwaan, 2001, Sources of the Slowly-Varying Component of Solar Microwave Emission and their Relationship with their Host Active Regions: Solar Physics, **199**, 2, 317–344, doi: 10.1007/BF00152730.

Thuillier, G., J. Claudel, D. Djafer, M. Haberreiter, N. Mein, S. M. L. Melo, W. Schmutz, A. Shapiro, C. I. Short, and S. Sofia, 2011, The Shape of the Solar Limb: Models and Observations: Solar Physics, **268**, 1, 125–149, doi: 10.1007/s11207-010-9664-7.

Trottet, G., J. P. Raulin, G. G. De Castro, T. Lüthi, A. Caspi, C. H. Mandrini, M. L. Luoni, and P. Kaufmann, 2011, Origin of the Submillimeter Radio Emission during the Time-Extended Phase of a Solar Flare: Solar Physics, **273**, 2, 339–361, doi: 10.1007/978-1-4614-4403-9_3.

Tsuchiya, A., and K. Takahashi, 1968. Spectrum of Slowly Varying Component of Solar Radio Emission on Millimeter Wavelengths: Solar Physics, **3**, 2, 346–348, doi: 10.1007/BF00155168.

Valio, A., P. Kaufmann, C. G. G. De Castro, J. P. Raulin, L. O. T. Fernandes, and A. Marun, 2013, POlarization Emission of Millimeter Activity at the Sun (POEMAS): New Circular Polarization Solar Telescopes at Two Millimeter Wavelength Ranges: Solar Physics, **283**, 2, 651–665, doi: 10.1007/s11207-013-0237-4.

Valio, A., E. Spagiari, M. Marengoni, and C. L. Selhorst, 2020, Correlations of Sunspot Physical Characteristics during Solar Cycle 23: Solar Physics, **295**, 9, 120, doi: 10.1007/s11207-020-01691-3.

Valle Silva, J. F., C. G. Giménez de Castro, C. L. Selhorst, J.-P. Raulin, and A. Valio, 2021, Spectral signature of solar active region in millimetre and submillimetre wavelengths: Monthly Notices of the Royal Astronomical Society, **500**, 2, 1964–1969, doi: 10.1093/mnras/staa3354.

Vestrand, W. T., D. J. Forrest, E. L. Chupp, E. Rieger, and G. H. Share, 1987. The Directivity of High-Energy Emission from Solar Flares. II. Solar Maximum Mission Observations: The Astrophysical Journal, **322**, 1010, doi: 10.1086/165796.

Wagner, W. J., 1984, Coronal Mass Ejections: Annual Review of Astronomy and Astrophysics, **22**, 267–289, doi: 10.1146/annurev.aa.22.090184.001411.

Wannier, P. G., G. J. Hurford, and G. A. Seielstad, 1983, Interferometric observations of solar limb structure at 2.6 millimeters: The Astrophysical Journal, **264**, 660–666, doi: 10.1086/160639.

Webb, D. F., and T. A. Howard, 2012, Coronal Mass Ejections: Observations: Living Reviews in Solar Physics, **9**, 3, doi: 10.12942/lrsp-2012-3.

White, S. M., A. O. Benz, S. Christe, F. F.rn.k, M. R. Kundu, G. Mann, Z. Ning, J. P. Raulin, A. V. R. Silva-Valio, P Saint-Hilaire, N. Vilmer, and A. Warmuth, 2011, The Relationship Between Solar Radio and Hard X-ray Emission: Space Science Reviews, **159**, 1-4, 225–261, doi: 10.1007/s11214-010-9708-1.

Wrixon, G. T., 1970, Solar Eclipse Measurements at 16 and 30 GHz. Nature, **227**, 1231–1232, doi: 10.1038/2271231a0.

Valio, A.: review manuscript conceptualization and writing; **Menezes, F.:** manuscript review, supply of Figures 2, 6, 7, and 8; **Silva, D.F.:** manuscript review, supply of Figures 10 and 12.

Received on August 08, 2022 / Accepted on July 25, 2023